

Spin polarization of quaternary $\text{Co}_2\text{Cr}_{1-x}\text{Fe}_x\text{Al}$ Heusler alloys

S. V. Karthik and A. Rajanikanth

Graduate School of Pure and Applied Sciences, University of Tsukuba, Tsukuba 305-8571, Japan

Y. K. Takahashi, T. Okhubo, and K. Hono^{a)}

National Institute for Materials Science, Tsukuba 305-0047, Japan

(Received 2 May 2006; accepted 16 June 2006; published online 2 August 2006)

Point contact Andreev reflection measurements of $\text{Co}_2\text{Cr}_{1-x}\text{Fe}_x\text{Al}$ Heusler alloys showed that the spin polarization P decreases with x from $P=0.62$ for $x=0.0$ to $P=0.54$ for $x=0.4$ and then increases slightly to $P=0.56$ for $x=1.0$. The deviation in P of the samples with $x=0.0$ and 0.4 from the theoretical predictions ($P>0.9$) can be accounted to the phase separation, whereas the deviation in P of the sample with $x=1.0$ from the theoretical predictions ($P=0.3$) suggests the lack of accuracy in density of state calculations. © 2006 American Institute of Physics.

[DOI: 10.1063/1.2245224]

Half-metallic ferromagnetic materials have been extensively investigated in the field of spintronics for realizing the spin-dependent devices with high magnetoresistance and spin injection into semiconductors. These materials possess a gap in the minority band (viz., semiconducting), while it exhibits metallic behavior in the majority band; in other words, the electrons at the Fermi level have a 100% spin polarization. The first materials that were theoretically predicted to be a half-metallic ferromagnet from the electronic band structure calculations were the $C1_b$ -type half-Heusler alloys, viz., NiMnSb and PtMnSb by de Groot *et al.*¹ in 1983. Subsequently, various other half-metallic ferromagnetic materials have been studied, such as CrO_2 ,² double perovskites $\text{Sr}_2\text{FeReO}_6$,³ pyrites CoS_2 ,⁴ and zinc-blende-type CrSb .⁵ Many studies on the magnetic tunnel junctions (MTJs) using the above materials have been carried out; however, large values of tunneling magnetoresistance (TMR) have not been reported at room temperature because of their low Curie temperature and some difficulties in MTJ fabrications. Currently, the $L2_1$ -type full-Heusler alloys are believed to be the most promising half-metallic ferromagnetic materials which exhibit both a high spin polarization and high Curie temperature.

Recently, Galanakis⁶ studied full-Heusler quaternary alloys such as $X_2Y_{1-x}Y'_xZ$, $(X_{1-x}X'_x)_2YZ$ and $X_2YZ_{1-x}Z'_x$ and found the possibility of obtaining half-metallic systems with predefined electronic and magnetic properties. Theoretical calculations on the electronic band structure of $B2$ -type and $L2_1$ -type $\text{Co}_2\text{Cr}_{1-x}\text{Fe}_x\text{Al}$ exhibit a half-metallic behavior for the lower concentration range of x . In addition, the Curie temperature (T_C) of the $\text{Co}_2\text{Cr}_{1-x}\text{Fe}_x\text{Al}$ alloy⁷ increases from 330 K for $x=0.0$ to 1170 K for $x=1.0$. Subsequently, $\text{Co}_2\text{Cr}_{1-x}\text{Fe}_x\text{Al}$ has been experimentally investigated and a large negative magnetoresistive effect of 30% at room temperature was observed by Block *et al.*⁸ for the $\text{Co}_2\text{Cr}_{0.6}\text{Fe}_{0.4}\text{Al}$ bulk alloy. Following this result, Inomata *et al.*⁹ prepared a spin-valve-type tunneling junction with a $\text{Co}_2\text{Cr}_{0.6}\text{Fe}_{0.4}\text{Al}$ electrode on thermally oxidized silica and reported TMR values of 27% and 19% at 5 K and room temperature, respectively. However, these values are signifi-

cantly lower than those expected from highly spin-polarized materials according to Julliere's formula, $\text{TMR}=2P_1P_2/(1-P_1P_2)$, where P_1 and P_2 are the spin polarizations of ferromagnetic electrodes.¹⁰ Kobayashi *et al.*⁷ investigated the phase equilibrium of the $\text{Co}_2\text{Cr}_{0.6}\text{Fe}_{0.4}\text{Al}$ bulk alloy and demonstrated that $A2$ and $L2_1$ phases coexist in the Co_2CrAl and $\text{Co}_2\text{Cr}_{0.6}\text{Fe}_{0.4}\text{Al}$ alloys at 773 K. These two phase states were not considered in the theoretical prediction of the spin polarization of the $\text{Co}_2\text{Cr}_{1-x}\text{Fe}_x\text{Al}$ alloys. Thus, a direct measurement of the spin polarization of these electrode materials is strongly desired to understand the disappointingly low TMR values obtained from the MTJs using the $\text{Co}_2\text{Cr}_{1-x}\text{Fe}_x\text{Al}$ alloys. In this study, we have investigated the microstructure, magnetic properties, and the spin polarization of $\text{Co}_2\text{Cr}_{1-x}\text{Fe}_x\text{Al}$ alloys by transmission electron microscopy (TEM), a vibrating sample magnetometer (VSM), and point contact Andreev reflection (PCAR) measurements.

Polycrystalline Co_2CrAl , $\text{Co}_2\text{Cr}_{0.6}\text{Fe}_{0.4}\text{Al}$, and Co_2FeAl alloy ingots were prepared by arc melting the constituent elements (purity of 99.9% or more) under an argon atmosphere. Melting was repeated several times to ensure chemical homogeneity, and Co_2CrAl and $\text{Co}_2\text{Cr}_{0.6}\text{Fe}_{0.4}\text{Al}$ samples were annealed at 773 K for 72 h to achieve thermodynamic equilibrium. The microstructures of the samples were observed by TEM. Energy filtered TEM images were acquired using Gatan imaging filter (GIF) Tridiem using the jump ratio method on Technai G2 F30 TEM. Magnetization curves were measured with a VSM. PCAR (Ref. 11 was used to measure the spin polarization P by fitting the experimental conductance-voltage curve using the modified version of the Blonder-Tinkham-Klapwijk (BTK) model.¹² The PCAR measurement was carried out using a Nb-tip/ $\text{Co}_2\text{Cr}_{1-x}\text{Fe}_x\text{Al}$ contact in liquid helium.

Figures 1(a)–1(c) show the selected area electron diffraction (SAED) patterns with the specimen along the $[01\bar{1}]$ zone axis and the TEM dark field images taken from the $(100)_{B2}$ reflection for Co_2CrAl , from the $(200)_{B2}$ reflection for $\text{Co}_2\text{Cr}_{0.6}\text{Fe}_{0.4}\text{Al}$, and from the $(100)_{B2}$ reflection for Co_2FeAl , respectively. The dark field images in Figs. 1(a) and 1(b) show that the alloys are phase separated into disordered $A2$ phase (darkly imaging region) and a $B2$ phase for Co_2CrAl and an $L2_1$ phase for $\text{Co}_2\text{Cr}_{0.6}\text{Fe}_{0.4}\text{Al}$. In the TEM dark field image of the Co_2FeAl alloy [Fig. 1(c)], $B2$ -type

^{a)}Also with Graduate School of Pure and Applied Sciences, University of Tsukuba.

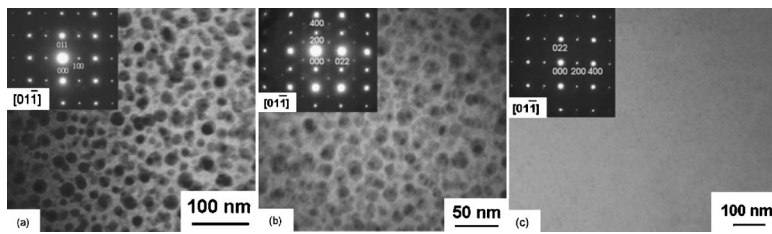


FIG. 1. $[01\bar{1}]$ selected area electron diffraction (SAED) patterns and TEM dark field images taken from the $B2$ (100) reflection spot for Co_2CrAl (a), $L2_1$ (200) spot for $\text{Co}_2\text{Cr}_{0.6}\text{Fe}_{0.4}\text{Al}$ (b), and $B2$ (100) spot for Co_2FeAl (c).

phase without any other precipitates can be observed. Note that the microstructures of these alloys are consistent with the phase diagram illustrated by Kobayashi *et al.*⁷ in which the alloys with less than $x=0.4$ are in the $A2+B2$ two phase region and the alloys with more than $x=0.7$ forms a single phase $B2$ structure and $L2_1$ -type single phase can be obtained after heat treatment.

The GIF elemental maps of Co and Cr in the $\text{Co}_2\text{Cr}_{0.6}\text{Fe}_{0.4}\text{Al}$ alloy annealed at 773 K for 72 h are shown in Fig. 2. The precipitates, i.e., the dark globules in the TEM dark field image corresponding to the $A2$ phase [see Fig. 1(a)] are enriched with Cr [as shown in Fig. 2(b)] and depleted with Co atoms [as shown in Fig. 2(a)]. The Fe and Al maps did not show any contrast with the GIF map. However, separate atom probe analysis has identified that Fe and Al were also rejected from the $A2$ phase, which will be reported elsewhere. This confirms that the compositions of the $L2_1$ and $A2$ phases shift to Co-rich and Cr-rich sides as predicted by the thermodynamic calculations. Similar microstructures of the Co_2CrAl alloy indicate that the composition of the $B2$ ordered matrix phase also shifts to a Co-rich composition from its stoichiometry.

The PCAR measurements were performed in liquid helium using superconducting Nb tips for the bulk $\text{Co}_2\text{Cr}_{1-x}\text{Fe}_x\text{Al}$ alloys to determine the spin polarization. Figures 3(a)–3(c) show the respective conductance-voltage curves for the $\text{Co}_2\text{Cr}_{1-x}\text{Fe}_x\text{Al}$ alloys with $x=0.0, 0.4$, and 1.0 with different contact resistances which were administered by varying the contact area mechanically. The contact resistances range from 20 to 40 Ω . All the curves can be fitted very well by the modified BTK model¹² as illustrated by the solid lines in the figures using three parameters: spin polarization (P), superconducting gap (Δ), and interfacial scattering barrier strength (Z). The values of P , Δ , and Z resulting from the fits are shown in the figures. Figure 3(d) shows the systematic variation of the fitted P with Z for the $\text{Co}_2\text{Cr}_{1-x}\text{Fe}_x\text{Al}$ alloys with $x=0.0, 0.4$, and 1.0 . The bulk spin polarization can thus be obtained by extrapolating the P vs Z curve to the limit of $Z=0$. By employing this method, the bulk spin polarizations for Co_2CrAl , $\text{Co}_2\text{Cr}_{0.6}\text{Fe}_{0.4}\text{Al}$, and Co_2FeAl have been estimated to be $P=0.62, 0.54$, and 0.56 , respectively, with an accuracy of $\pm 2\%$. The P value obtained

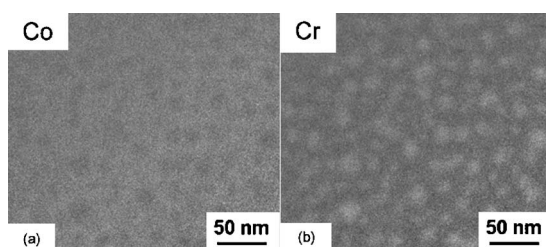


FIG. 2. GIF jump ratio images of Co and Cr in the $\text{Co}_2\text{Cr}_{0.6}\text{Fe}_{0.4}\text{Al}$ alloy annealed at 773 K for 72 h.

for the $\text{Co}_2\text{Cr}_{0.6}\text{Fe}_{0.4}\text{Al}$ alloy is higher than $P=0.492$ reported by Auth *et al.*¹³

The total magnetic moment per unit cell, M_t , measured at room temperature and P for the $\text{Co}_2\text{Cr}_{1-x}\text{Fe}_x\text{Al}$ alloys are shown in Fig. 4. The open squares and closed circle represent M_t and P , respectively. The dashed line and the solid line show the theoretical prediction⁸ and the experimental results, respectively. Figure 4 shows that M_t increases with increasing x similar to the Slater-Pauling curve $M_t=Z_t-24$.¹⁴ The deviation of M_t from the Slater-Pauling curve becomes more significant at a lower concentration range of $x=0.4$ due to the phase separation into a Co-enriched matrix phase and a Cr-enriched globular precipitate [as shown in Fig. 2(b)]. The decrease in the total magnetic moment resulting from the Co–Cr disorder was reported in the Co_2CrAl alloy.¹⁵ This is because the Co–Cr-type disorder lowers the total magnetic moment due to the antiferromagnetic coupling of the antiseite Cr with the first nearest neighboring ordinary-site Cr. On the other hand, the value of P obtained by the PCAR measurement decreases from 0.62 to 0.56 with increasing x . From the first principles calculations,¹⁵ the spin polarization of the $\text{Co}_2\text{Cr}_{1-x}\text{Fe}_x\text{Al}$ alloy with the ordered $L2_1$ structure and the disordered $B2$ structure gradually decreases with increasing x from $P>0.9$ up to $x=0.35$ to about $P=0.3$ at $x=1.0$, which is mainly due to the appearance of the Fe $3d$ minority density of states (DOS) at the Fermi level. In addition, the Co–Cr-type disorder of just about 10% for the Co_2CrAl alloy was reported to reduce the spin polarization by more than 30%. Therefore, the deviation in the spin polarization of the Co_2CrAl and $\text{Co}_2\text{Cr}_{0.6}\text{Fe}_{0.4}\text{Al}$ alloys by the PCAR measurements from the theoretical predictions can be accounted to

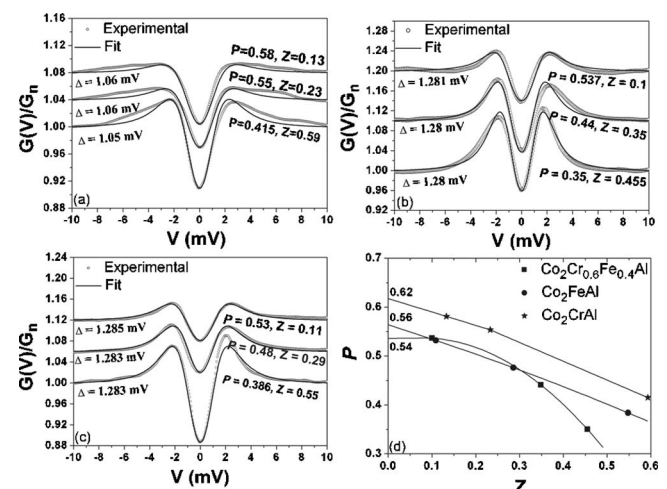


FIG. 3. Measured conductance $[G(V)/G_n]$ vs voltage (V) curves for the Nb/ $\text{Co}_2\text{Cr}_{1-x}\text{Fe}_x\text{Al}$ point contacts with $x=0.0$ (a), $x=0.4$ (b), and $x=1.0$ (c) for different contact resistances (open circles). Solid lines are the fits to the data using the modified BTK model using the P , Z , and Δ values as indicated in the figure. Bulk P value was obtained by extrapolating P to $Z=0$ (c).

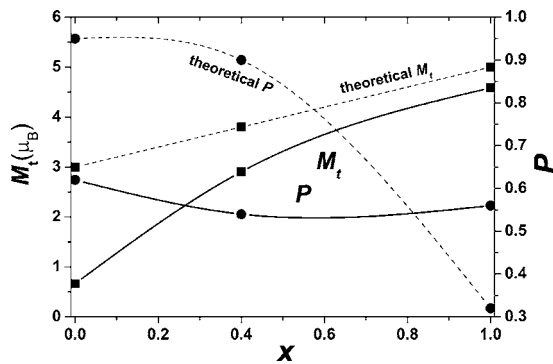


FIG. 4. Concentration dependence of the saturation magnetization M_t and the spin polarization (P) for the $\text{Co}_2\text{Cr}_{1-x}\text{Fe}_x\text{Al}$ alloys; Solid and dashed lines with open squares correspond to the experimental and theoretical M_t and that with closed circles correspond to the experimental and theoretical P with increasing x . Theoretical P was incorporated from Ref. 17.

the presence of phase separation into the $A2$ phase and the $B2$ or $L2_1$ phase as seen in the microstructure of these alloys [see Figs. 1(a) and 1(b)]. Note that the spin polarization of Co_2FeAl obtained by the PCAR measurement ($P=0.56$) is higher than the theoretical prediction¹⁵ ($P=0.3$) as shown in Fig. 4. However, there are some recent reports on the DOS calculations of Co_2FeAl suggesting 100% spin polarization with a band gap at the Fermi level^{16,17} for the minority states. In addition to this, by considering the electron-electron correlation of Co_2FeSi with modified DOS calculations, 100% spin polarization has been theoretically predicted.¹⁸ Such similar calculations can throw light in understanding the high spin polarization obtained for Co_2FeAl .

From the experimental values of P , the upper limit of the TMR values expected from MTJs using a Co_2CrAl , $\text{Co}_2\text{Cr}_{0.6}\text{Fe}_{0.4}\text{Al}$, and Co_2FeAl electrode will be 90%, 75%, and 78%, respectively, if the other electrode is CoFe ($P=0.5$). The TMR values reported by Inomata *et al.*¹⁹ for MTJs using $\text{Co}_2\text{Cr}_{0.6}\text{Fe}_{0.4}\text{Al}$ and Co_2FeAl electrodes were 70% and 77% at 5 K, closely matching our results. The TMR value of 77% of the MTJ using Co_2FeAl again indicates that the theoretically predicted P for Co_2FeAl ($P=0.3$) is underestimation. On the other hand, the TMR values for the MTJ using the Co_2CrAl electrode of 13% is much lower than the upper limit estimated from the experimental value of $P=0.6$. This difference could be attributed to higher surface roughness and oxidation, Co–Cr disorder, and rough interface. The present work suggests that a different type of Heusler alloy with a higher spin polarization must be sought to achieve higher TMR values exceeding 100% at room temperature.

In summary, the microstructure, magnetic properties, and spin polarization of $\text{Co}_2\text{Cr}_{1-x}\text{Fe}_x\text{Al}$ alloys were investigated. Phase separation into a Cr-enriched $A2$ phase and a Co-

enriched $B2$ or $L2_1$ matrix occurs in the Co_2CrAl and $\text{CoCr}_{0.6}\text{Fe}_{0.4}\text{Al}$ alloys in equilibrium. The deviation of the saturation magnetization M_t from the Slater-Pauling curve becomes significant for the Co_2CrAl and $\text{CoCr}_{0.6}\text{Fe}_{0.4}\text{Al}$ alloys due to the phase separation. From the PCAR measurements, the spin polarizations of $\text{Co}_2\text{Cr}_{1-x}\text{Fe}_x\text{Al}$ alloys were found to be $P=0.62$ at $x=0.0$, $P=0.54$ at $x=0.4$, and $P=0.56$ at $x=1.0$ with an accuracy of $\pm 2\%$. The deviation in the spin polarization of the Co_2CrAl and $\text{Co}_2\text{Cr}_{0.6}\text{Fe}_{0.4}\text{Al}$ alloys from the theoretical predictions can be accounted to the $A2$ and $B2/L2_1$ two phase microstructures. The experimentally determined $P=0.56$ for Co_2FeAl indicates the necessity of further refinement of the prediction of the spin polarization by DOS calculations.

This work was in part supported by the Ministry of Education, Science, Sports and Culture of Japan, Grant-in-Aid for Scientific Research (B), 17360346, 2005. The authors thank Asano at Nagoya University and Mitani at Institute for Materials Research, Tohoku University, for valuable advice in the point contact Andreev reflection measurement and Inomata for discussion.

- ¹R. A. de Groot, F. M. Mueller, P. G. van Engen, and K. H. J. Bushow, *Phys. Rev. Lett.* **50**, 2024 (1983).
- ²S. P. Lewis, P. B. Allen, and T. Sasaki, *Phys. Rev. B* **55**, 10253 (1997).
- ³H. Kato, T. Okuda, Y. Okimoto, Y. Tomioka, K. Oikawa, T. Kamiyama, and Y. Tokura, *Phys. Rev. B* **69**, 184412 (2004).
- ⁴T. Shishidou, A. J. Freeman, and R. Asahi, *Phys. Rev. B* **64**, 180401 (2001).
- ⁵I. Galanakis and P. Mavropoulos, *Phys. Rev. B* **67**, 104417 (2003).
- ⁶I. Galanakis, *J. Phys.: Condens. Matter* **16**, 3089 (2004).
- ⁷K. Kobayashi, R. Y. Umetsu, R. Kainuma, K. Ishida, T. Oyamada, A. Fujita, and K. Fukamichi, *Appl. Phys. Lett.* **85**, 4684 (2004).
- ⁸T. Block, C. Felser, G. Jakob, J. Ensling, B. Muhling, P. Gutlich, and R. J. Cava, *J. Solid State Chem.* **176**, 646 (2003).
- ⁹K. Inomata, S. Okamura, and N. Tezuka, *J. Magn. Magn. Mater.* **282**, 269 (2004).
- ¹⁰M. Julliere, *Phys. Lett.* **54A**, 225 (1975).
- ¹¹R. J. Soulen, Jr., J. M. Byres, M. S. Osofsky, B. Nadgorny, T. Ambrose, S. F. Cheng, P. R. Broussard, C. T. Tanaka, J. Nowak, J. S. Moodera, A. Bary, and J. M. D. Coey, *Science* **282**, 85 (1998).
- ¹²G. E. Blonder, M. Tinkham, and T. M. Klapwijk, *Phys. Rev. B* **25**, 4515 (1982).
- ¹³N. Auth, G. Jakob, T. Block, and C. Felser, *Phys. Rev. B* **68**, 024403 (2003).
- ¹⁴I. Galanakis, P. H. Dederichs, and N. Papanikolaou, *Phys. Rev. B* **66**, 174429 (2002).
- ¹⁵Y. Miura, K. Nagao, and M. Shirai, *Phys. Rev. B* **69**, 144413 (2004).
- ¹⁶G. H. Fecher, H. C. Kandpal, S. Wurmehl, J. Morais, H. Lin, H. Elmers, G. Schonhense, and C. Felser, *J. Phys.: Condens. Matter* **17**, 7237 (2005).
- ¹⁷S. Wurmehl, G. H. Fecher, K. Kroth, F. Kronast, H. A. Durr, Y. Takeda, Y. Saitoh, K. Kobayashi, H. Lin, G. Schonhense, and C. Felser, *J. Phys. D* **39**, 803 (2006).
- ¹⁸S. Wurmehl, G. H. Fecher, H. C. Kandpal, V. Ksenofontov, H. Lin, J. Morais, and C. Felser, *Phys. Rev. B* **72**, 184434 (2005).
- ¹⁹K. Inomata, S. Okamura, A. Miyazaki, M. Kikuchi, N. Tezuka, M. Wojcik, and E. Jedryka, *J. Phys. D* **39**, 816 (2006).